The International Journal of Advanced Manufacturing Technology (2020) 106:5317–5331
https://doi.org/10.1007/s00170-019-04910-9

ORIGINAL ARTICLE

Electromagnetic heating for adhesive melting in CFRTP joining: study, analysis, and testing

L. Nele[1] · B. Palmieri[1]

Received: 11 March 2019 / Accepted: 30 December 2019 / Published online: 6 February 2020

Abstract
Induction heating of thermoplastic composites is a suitable and promising technique, due to the very short heating time and the possibility of generating the heat at the interface between the adherends compared with other heating technologies, i.e. owen heating or hot melt gun manual deposition. The aim of this work is to study the electromagnetic induction heating in adhesive bonding of thermoplastic matrix composite materials, when a hot-melt thermoplastic adhesive, Prodas, is used. A numerical model for studying the effect of the process parameters, such as current intensity, maximum temperature and holding time at maximum temperature, has been developed. Experimental tests validated the results of the numerical model; also, the mechanical properties of the adhesive joints were evaluated by short beam shear test and single lap shear tests to define the values of technological parameters allowing for the better joint strength. Moreover, ANOVA analysis was employed to evaluate the most significant parameter which affected the mechanical properties, highlighting the optimum process parameters.

Keywords Automotive · FE-Modelling · Induction heating · Thermoplastic composites

1 Introduction

The birth and the subsequent development of carbon fibre reinforced thermoplastic (CFRTP) composite are a direct consequence of automotive industrial research of materials that combine high mechanical characteristics, with a very low weight [1].

An obstacle to the wide application of these materials is related to the high viscosity of the resin and the limited deformation allowed by the reinforcing fibres. These aspects represent a limitation for the geometry of the parts to be produced so that assembling of many parts is still required in industrial manufacturing of these materials. There are several techniques for joining thermoplastic matrix composites, such as mechanical fastening, fusion bonding or welding, reviewed by Ageorges et al. [2], and adhesive and solvent bonding.

✉ L. Nele
luigi.nele@unina.it

[1] Department of Chemical, Materials and Industrial Production Engineering, University of Naples Federico II, P.le Tecchio 80, 80125 Naples, Italy

Mechanical fastening, such as riveting and bolting, involves several disadvantages, such as stress concentrations, delamination during drilling [3], different thermal expansion of fasteners relative to composite, possible galvanic corrosion, additional weight and problem of heat generation [4]. Adhesive bonding could be a suitable joining technique for composite structure. Adhesive bonding has allowed the development of construction of lighter structures, replacing the rivets in the joints, above all in the automotive industry, and, moreover, has permitted avoiding welding where temperature gradients could damage materials [5].

The mechanical properties of two surfaces joined with an adhesive depend on many parameters, such as their pretreatment [6], their wettability by the liquid adhesive and adhesion forces [7], bonding between the substrate and the solidified adhesive, and, by the cohesion, bonding forces acting within the adhesive itself.

Hot-melt adhesives are made up of adhesives based on thermoplastic polymers, elastomers, (polyurethanes) and thermoplastic terpolymers and styrene-olefins, ethylene or propylene or butadiene: these polymers liquefy for heating and solidify for subsequent cooling.

As soon as the softened hot-melt adhesive is put in contact with the surfaces to be joined, a heat transfer gradient is generated throughout the substrate's area. The high difference

between the masses of the two materials, adhesive and adherends, allows to rapidly decrease the temperature to the value at which the adhesive restores its solid state by acquiring a cohesive force that holds the two adherends' surfaces firmly bonded together.

Several methods can obtain the heat required for the liquefaction of hot-melt adhesive.

In this work, an alternative heating process for adhesively bonded joints, based on induction heating (IH), was investigated. Electromagnetic induction heating is a process that requires no contact between the induction coil and the workpiece, and, if the inductor is well designed, no heating is produced outside of the working area. This process is not an innovative technology, as is very frequently applied for heating magnetic susceptible metals [8]. When an electrical conductor is placed in an alternating electromagnetic field, generated by an induction coil, several physical phenomena occur, e.g. eddy currents flowing [9]. The eddy currents' flow, according to Joule's first law, causes the material heating.

Usually, thermoplastic adhesives are neither magnetic nor conductive, but it is possible to heat the adhesive by induction heating the adherends.

Moreover, recently, this technology has also been employed for heating carbon fibre-based composites; in fact, induction joining of thermoplastic carbon fibre reinforced polymer composites (CFRTP) is proving itself to be a very effective method.

Several authors investigated the principle of induction heating of carbon fibre reinforced thermoplastics. Miller et al. [10] and Fink [11] observed that the heating mechanism is based on eddy current induced in the workpiece, provided conductive fibre arrays form closed-loop circuits, e.g. fabrics or cross-plies. Yarlagadda et al. [12] have investigated three different possible heating mechanisms: Joule losses, which occur within the fibres, dielectric hysteresis, and contact resistance, which occurs at the fibres crossovers, to identify dominant heating mechanisms during induction processing of conductive fibre reinforced composites.

Recently, some authors have investigated the possibility to apply IH for the thermosetting adhesive curing process: Sanchez et al. [13] have investigated an IH curing process using CFRTP adherends and a two-component epoxy paste adhesive. In this study, they demonstrated how in this process the energy consumption is approximately 25% less than traditional curing techniques.

Additionally, Severijns et al. [14] have studied the curing and mechanical behaviour of a mix of iron particles and two component epoxy paste adhesive, demonstrating that adding iron particles to the adhesive results in a reduction of the lap-shear strength.

Induction heating can be considered a very complicated multiphysics process requiring understanding both the electromagnetic and the heat transfer phenomena in the laminates. In fact, the prediction of the temperature evolution during induction heating is of utmost importance to optimise the process parameters and to obtain high strength joints.

Recently, O'Shaughnessy et al. [15] have developed a three-dimensional finite element model of the induction welding of CFRTP; in their study, they have considered a stainless steel wire mesh, named heating element, located at the interface of the adherends, demonstrating that the presence of this kind of element does not affect the mechanical characteristics of the joint.

Instead, in this work, thanks to substrate's heating by electromagnetic induction, the adhesive was heated up to the liquefying temperature range, at which the adhesive is liquid and hence can wet the adherends.

The present study has two objectives. The first objective is the development of a numerical model capable of predicting the temperature increase of the hot-melt adhesive and the composite adherends by induction heating.

As evidenced by careful bibliographic research, there is a lack of studies concerning a numerical model predicting the heating trend during the curing process of a hot-melt thermoplastic adhesive to join carbon fibre reinforced thermoplastic (CFRTP).

Experimental activities were also performed to validate the developed model.

The second objective is optimising the different parameters that affect the final performances of the induction-heated adhesive bonding. Mechanical tests according to two different ASTM standard methods, single lap shear and short beam shear tests, confirmed the effectiveness of the optimised parameters. The single lap joint shear (SLS) test is one of the most used methods to measure the joint performance [16]; the principal advantages of this test method are its simplicity and low cost, but several disadvantages characterise it.

In fact, as demonstrated by Luo and Tong [17], the stress distribution is strongly non-uniform and depends on the geometry, as reported by Silva et al. [18]. De Castro and Keller [19] demonstrated how the joint strength depends on the overlap length; Reis et al. [20] investigated the effect of the rigidity of the adherends on joint strength.

The short beam shear (SBS) test has been used for evaluating composite laminates, and as demonstrated by Pahr et al. [21], the SBS test is more accurate than the SLS.

A comparative study of the two different standard methods, SLS and SBS, is finally conducted. In particular, the surface of the fracture and the results obtained from the SLS tests are compared with those obtained from the SBS tests.

The level of importance of the process parameters is determined by using analysis of variance (ANOVA). The optimum process parameter combination was obtained by using the analysis of the mechanical test results.

Analysis of variance (ANOVA) was also applied to analyse the maximum significant aspects for the induction heating curing process, using electromagnetic induction heating.

2 Materials and methods

2.1 Materials

The study on the process parameters for the induction bonding was carried out on carbon fibre reinforced polyamide (CF-PA66): Tepex® Dynalite 202-C200 (9)/50% (PA6 50% carbon fibres), produced by Tencate. Prodas-1400 (Beardow Adams) was used as a thermoplastic adhesive.

The Prodas-1400 (hot-melt polyolefin) is a synthetic polymer-based adhesive allowable for assemblies where good cohesive strength and longer open time than other hot-melt adhesives (usually characterised by an open time of less than 30 s) are required.

2.2 Specimens

The joint mechanical characteristics were evaluated using short beam shear strength test and single lap joint shear test. According to ASTM's test methods, the specimens had the following dimensions:

- For ASTM D2344 [22]: 40 × 12 mm and thickness of 2 mm and total overlap
- For ASTM D5868 [23]: 100 × 25 mm and thickness of 2 mm and 25 × 25 overlap

The specimens were cut into single specimens, as prescribed by the ASTM's test methods, and then assembled and cured individually.

The adhesive, in the form of film, was cut with the dimension of the overlap zone, according to the ASTM's applied:

- For ASTM D2344, 40 × 12 mm and thickness of 1 mm
- For ASTM D5868, 25 × 25 mm and thickness of 1 mm

Figure 1 shows the load configurations and the dimensions of the specimens for the two different testing methods.

Besides, in order to compare the traditional method with the induction-heated adhesive bonding, a non-induction-cured samples were realised by providing the melted adhesive on the overlap zone of one of the adherends and subsequently coupling the other one adherend. The deposition of the adhesive, Prodas-1400, was realised using a manual applicator of adhesive hot-melt, set at the nozzle temperature of 185 °C.

To obtain a constant thickness of adhesive at 1 mm, the joint realised was positioned in a specific tool where a constant pressure acts for 2 min, the time during which the adhesive acquire cohesive force.

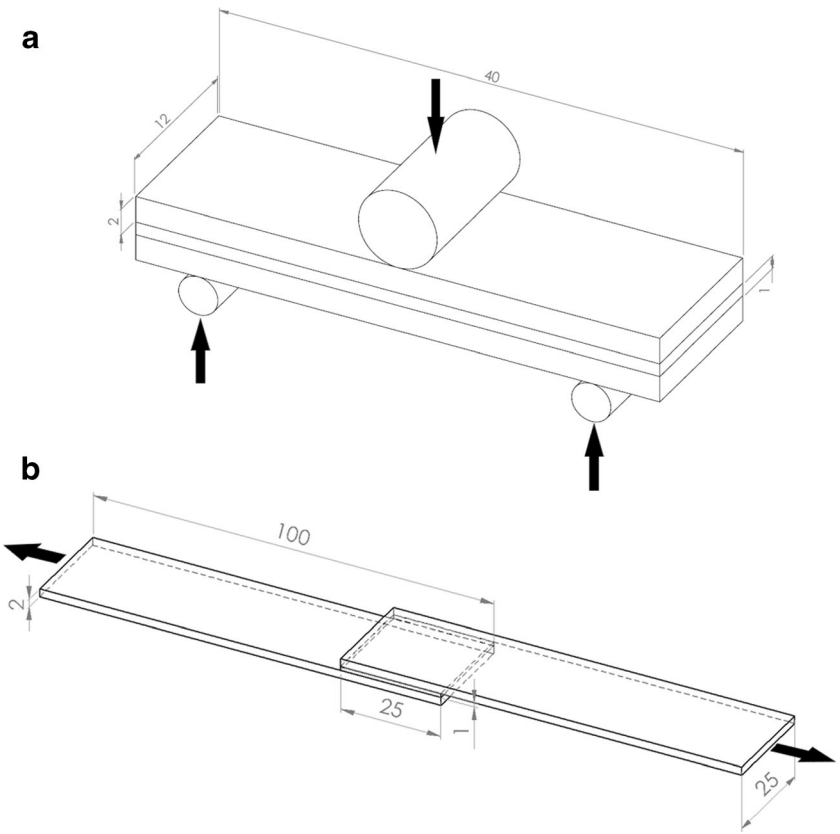

Fig. 1 Configuration and dimensions for **a** short beam shear strength test and **b** single lap joint shear test

2.3 Experimental set-up

The authors have considered the effect of three process parameters on the induction heating:

- The current intensity, to set the power
- The maximum temperature at the interface between adherends
- The holding time at maximum temperature

Each of these parameters was varied in its range of value, while the others were kept constant. The simulation cycle was designed using the DOE (design of experiment), taking into account the current generator characteristics to be used for the experimental phase, totalling 27 different cases.

In Table 1 are reported the different values of the process parameters imposed.

Because of the not uniformity of heating due to the edge effect that has been reported in previous studies [24], it was decided to vary the holding time, to homogenise the temperature over the adhesion interface area.

The choice of the three maximum temperature values depends on the Prodas adhesive liquefying temperature, which varies between 175 °C and 195 °C.

The induction heating equipment used is an EGMA 30R unit, designed and developed by Felmi (Italy). The generator can vary the frequency by 100–280 kHz, depending on the coil geometry and the current; the power can be tuned to 30 kW, ranging from 20% to 100%.

In this research, during the experimental tests, a "Spiral of Archimedes"-shaped induction coil was used, and the same geometry was modelled in the software; Fig. 2 shows the geometry of coil used. The material of the coil is electrolytic copper, and the operating frequency was kept constant at 145 kHz.

The current generator allows temperature control in a specific point of the specimen, appropriately chosen. In particular, the control is based on a pyrometer SKS-T14-09. This kind of system has a temperature range between −32 °C and 900 °C. It

Table 1 Summary of all simulations performed

Current (A)	Maximum temperature (°C)	Holding time (s)
10 (I_1)	175 (T_1) 185 (T_2) 195 (T_3)	10 (t_1), 20 (t_2), 30 (t_3)
17 (I_2)	175 (T_1)	10 (t_1)
	185 (T_2)	20 (t_2)
	195 (T_3)	30 (t_3)
24 (I_3)	175 (T_1)	10 (t_1)
	185 (T_2)	20 (t_2)
	195 (T_3)	30 (t_3)

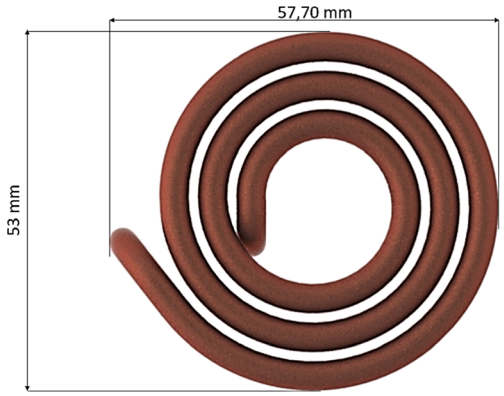

Fig. 2 Coil's shape and dimensions

utilises a silicon cell detector and operates at short wavelengths around 1.0 μm where emissivity errors are minimised. It has a fast response time of 5 ms. By reading the temperature value, it changes the current of the generator to keep the temperature constant once the imposed maximum temperature value is reached.

The authors decided to choose the point that experienced the maximum temperature according to preliminary experimental measurements. This point is located close to the adhesive area on the lateral side of the specimen, as reported in Fig. 3b.

For the correct measure of the temperature, it is necessary to know the value of the specimen's material emissivity; for carbon-carbon composite specimens, the emissivity is 0.8 [25]. The authors have verified that this value is suitable also for the material used in this work, using a thermocouple and calibrating the pyrometer emissivity value on the thermocouple reading.

The specimens were placed on an Ertalon's support, which was also considered in the numerical simulation, with the coil under the support.

As reported above, to measure the mechanical performance of the induction-cured adhesive, mechanical tests were performed, according to single lap joint shear test [23] and short beam shear strength test [22]. The tests were performed on a universal MTS Criterion Model45 dynamometer with a load cell of 100 kN.

For each series, a minimum of five specimens was tested.

3 Numerical model

Finite element simulations using JMAG Designer software were carried out coupling electromagnetic and energy balance differential equations to calculate the temperature distribution.

Mathematical equations describing the electromagnetic part are based on Maxwell's equations; a quasi-static approximation was used [26]. According to this approximation, Ampere's law can be written as:

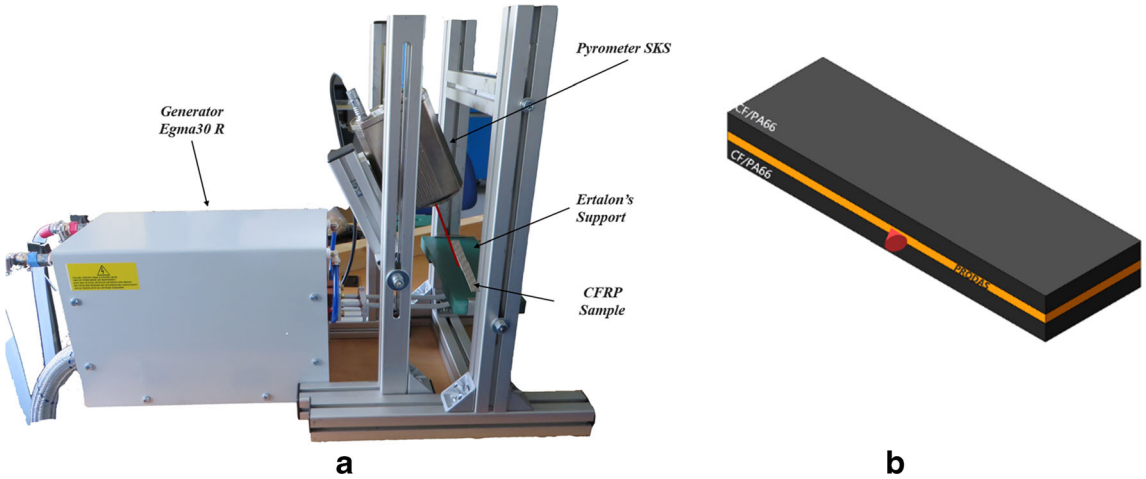

Fig. 3 **a** Experimental set-up; **b** the reported surface is controlled using an optical pyrometer and is the set point adopted for the control of the induction bonding equipment

$$\nabla \times H = \sigma(E + v \times B) \tag{1}$$

where (H) is the intensity of the magnetic field, (B) the magnetic flux density and (E) is the intensity of the electric field.

Considering that the workpiece and the coil are both static, the term $v \times B$ can be considered equal to zero.

The solved equations in 3D are:

$$\left(i\omega\sigma - \omega^2\,\varepsilon_0\varepsilon_r\right)\begin{pmatrix} A_x \\ A_y \\ A_z \end{pmatrix} + \begin{pmatrix} \frac{\partial H_z}{\partial y} - \frac{\partial H_y}{\partial z} \\ \frac{\partial H_x}{\partial z} - \frac{\partial H_z}{\partial x} \\ \frac{\partial H_y}{\partial x} - \frac{\partial H_x}{\partial y} \end{pmatrix} = \begin{pmatrix} J_{ex} \\ J_{ey} \\ J_{ez} \end{pmatrix} \tag{2}$$

$$\begin{pmatrix} B_x \\ B_y \\ B_z \end{pmatrix} = \begin{pmatrix} \frac{\partial A_z}{\partial y} - \frac{\partial A_y}{\partial z} \\ \frac{\partial A_x}{\partial z} - \frac{\partial A_z}{\partial x} \\ \frac{\partial A_y}{\partial x} - \frac{\partial A_x}{\partial y} \end{pmatrix} \tag{3}$$

where (J_e) is the external electric current density, (A) the magnetic potential, $\varepsilon_0$the permittivity of free space, $\varepsilon_r$the relative permittivity and σ the electric conductivity of carbon fibres.

The value of angular frequency, ω, of the magnetic field, depending on the frequency of the magnetic field f is $\omega = 2\pi f$.

These equations must be coupled with the constitutive equations of the electric and magnetic field (4) (5):

$$D = \varepsilon_0\varepsilon_r E \tag{4}$$

$$B = \mu_0\mu_r H \tag{5}$$

where D represents the electric displacement field, $\mu_0$the magnetic permeability of free space and μ_r the relative permeability.

The electromagnetic field manifests itself physically through heat generation due to the Joule effect; the heat is then distributed throughout the workpiece.

The energy balance is given by:

$$\rho C_p \frac{\partial T}{\partial t} - \nabla(\lambda \nabla T) = Q \tag{6}$$

In particular:

$$\rho C_p \frac{\partial T}{\partial t} = \frac{\partial}{\partial x}\left(k_x\left(\frac{\partial T}{\partial x}\right)\right) + \frac{\partial}{\partial y}\left(k_y\left(\frac{\partial T}{\partial y}\right)\right) + \frac{\partial}{\partial y}\left(k_z\left(\frac{\partial T}{\partial z}\right)\right) + Q \tag{7}$$

where ρ is the density, $C_p$is the specific heat, T is the temperature, k is the thermal conductivity along with the three directions and Q is the heat source, generated by eddy currents:

$$Q = \frac{1}{\sigma}\left|J_g\right|^2 \tag{8}$$

where J_g is the density of the generated eddy currents.

The heat generation caused by the magnetic field, generated by an alternate current which flows in a coil, was simulated using two modules, *FQ* (time-harmonic magnetic) and *HT* (steady/transient thermal); the assumed boundary conditions for both used modules (*FQ-HT*) were as follows:

- For the *FQ* module, the boundary conditions assigned were:

  – Assigning the current value to the coil
  – The electrical insulation to the upper surface of the air environment

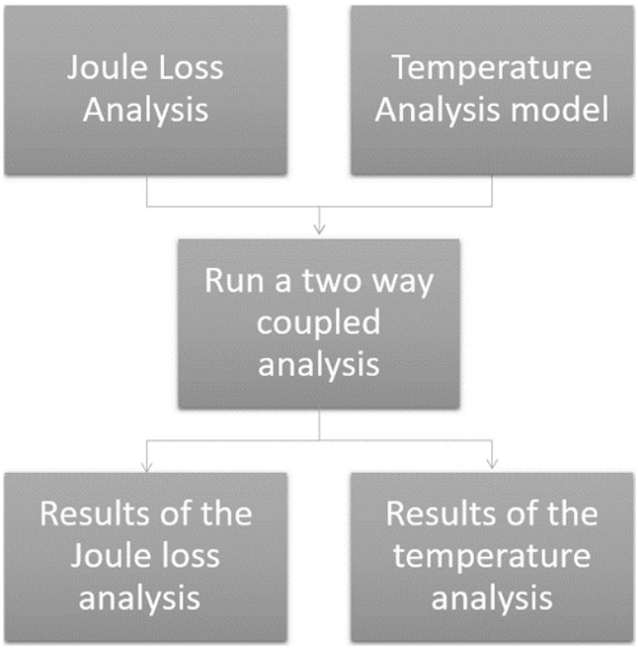

Fig. 4 Pattern of the model

– The magnetic insulation to the remaining surfaces of the air environment and external surfaces
– The continuity condition to all the remaining surface of the model

• For the *HT* module, the boundary conditions assigned were:

– The initial temperature is assigned to 20 °C
– Allocation of thermal flow to the surfaces of natural convection ($h = 5\ W/m^2K$)
– Assignment of the isolation/symmetry condition
– The continuity condition to all the remaining surface of the model

The software divides the physical phenomenon analysis into two analyses. The first one is related to the joule loss model, where a magnetic field analysis is used to handle the phenomenon produced by the eddy current and the magnetic field in the workpiece when current flows through the coil.

This analysis aims to obtain a distribution of Joule effect losses within the specimens, which renders it a source of heat in the analysis of electromagnetic induction heating.

The second one is the temperature analysis model, where the thermal analysis is used for the heat transfer phenomenon that occurs within the workpiece.

Figure 4 shows the pattern of the simulation model developed. The model was developed for each analysis. In this case, two models were defined for the joule loss analysis and the temperature analysis. After the models' tuning, a two-way coupled analysis was completed iteratively using the results of the Joule loss analysis for the processing of the thermal analysis and vice versa. Thermal analysis results were used to know the temperature trend during the process in the adherends and the adhesive.

Notes on how to develop each model are given below:

• For the Joule loss analysis model, a magnetic field/3D frequency analysis to obtain the joule loss is used.
• For the temperature analysis model, the heat generation distribution references the joule loss distribution obtained from the joule loss analysis.

The same setting values for the mesh generation were used in both the analysis model. In the temperature analysis model, it was set the heat source conditions to import the joule loss distribution data obtained from the joule loss analysis via a two-way coupling. Once the CAD model, realised in dedicated software, has been imported (Fig. 5) in JMAG, the electrical and magnetic properties of the materials of all components have been set (Table 2).

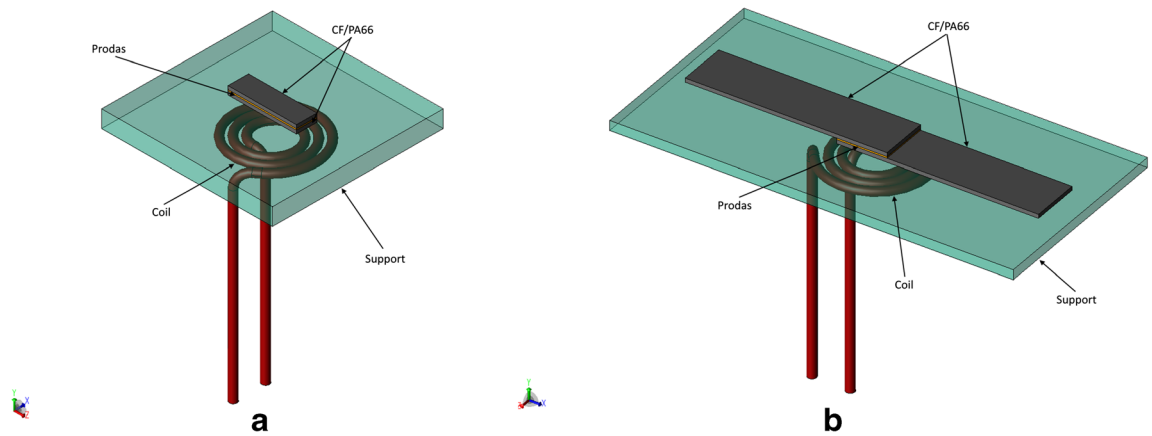

Fig. 5 **a** CAD model of short beam shear strength test; **b** CAD model of single lap joint shear test

Table 2 Input parameters of the FE model for CFRP, Ertalon's support and Prodas

Parameter	CFRP	Ertalon	Prodas
Heat capacity at constant pressure (C)	1000 (J/Kg*K)	1460(J/Kg*K)	1380(J/Kg*K)
Relative electrical permittivity (ε_r)	80	1	1
Thermal conductivity (k)	3.5 (W/m*K)	0.2 (W/m*K)	0.15 (W/m*K)
Relative magnetic permeability (μ_r)	1	1	1
Electrical conductivity (σ)	2×10^4 1/(Ω*m)	1×10^{-5} [1/(Ω*m]	1×10^{-5} [1/(Ω*m]
Density (ρ)	1.4 (g/m^3)	1.2 (g/m^3)	0.98 (g/m^3)

The value of the current imposed in the model has been set according to the trend shown in the graphic reported in Fig. 6, to keep constant the maximum temperature during the holding time.

4 Results and discussion

All the reported results were obtained from the simulations performed using the method previously described.

By using the Plot Parameters command in Project Manager, it is possible to choose the physical parameter to display, such as the temperature, and it is possible to monitor the evolution of their magnitude by choosing to visualise the value at a precise instant and for a known geometric entity, such as a point, or a line, or an area.

In the present case, it was chosen to extrapolate the temperature trend within the adhesive, as the technological objective is to reach the temperature of liquefying.

In Fig. 7, the trend of temperature for the case of 10 A current and holding time of 30 s is reported. The maximum temperature values are 175, 185 and 195 °C, as previously reported.

Figure 8 shows the evolution of the temperature in the adhesive layer. Figure 8(a) shows the temperature distribution just when the maximum temperature was reached, while Fig. 8(b) shows the temperature distribution after 30 s.

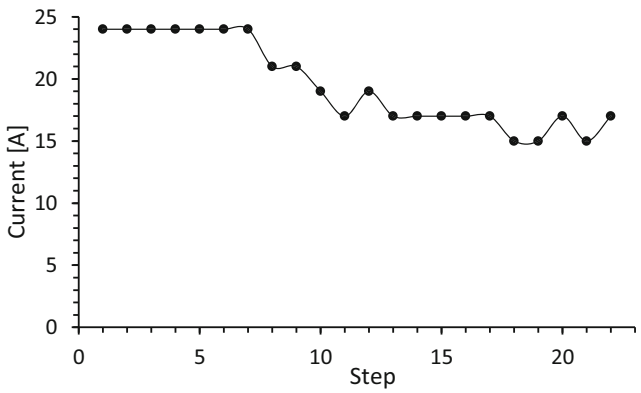

Fig. 6 Current values set

Figure 8 also shows how the hottest point in the adhesive layer moves from the outer edge inwards, allowing a more uniform temperature distribution.

The simulation has allowed to better understand the temperature distribution at the interface between CFRTP specimens and thermoplastic adhesive. Moreover, as is evident from Fig. 9, it also considers the heat transfer between the specimen and Ertalon's support.

4.1 Correlation

The numerical model was validated comparing the experimental temperature, measured at the joint interface during the induction bonding process, with the numerical model results.

The feedback, for heating control of the induction bonding, is given by a single point temperature measurement obtained using a pyrometer (SKS), implemented on the current generator as previously reported. As previously stated, it is crucial to control the maximum temperature to avoid the degradation, or even the burning, of the adhesive.

The results of the model were compared with the experimental measurements at the joint interface during the induction bonding process, and, as shown in Fig. 10, they fit the experimental results with outstanding accuracy.

4.2 Joint characteristics

Following the induction bonding tests, the mechanical characterisation was carried out to verify the effectiveness of the selected parameters.

The tests were performed using a universal MTS Criterion Model45 dynamometer with a load cell of 100 kN.

The standards test used, as described above, are the ASTM D2344 and D5868; the results of these tests are reported in Table 3. The values shown were obtained by averaging over five tests.

The strength of single lap joints and the interlaminar shear strength were characterised by satisfactory performance comparable with the results of the non-induction-cured sample.

The maximum values for both standards with the corresponding process parameters are reported in Table 4; additionally, these values are compared with the reference samples.

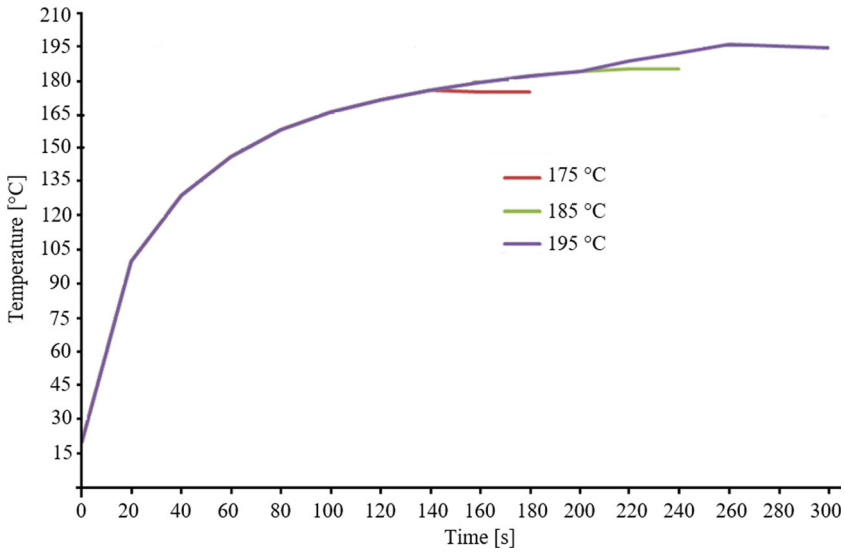

Fig. 7 Profile temperature

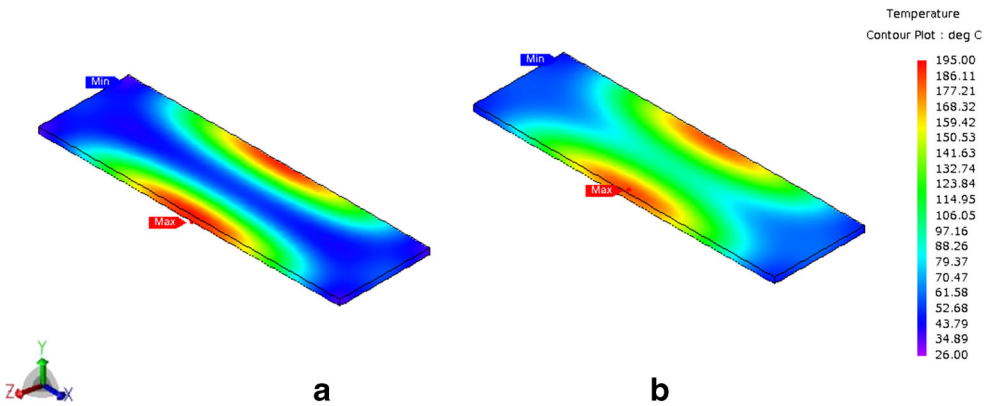

Fig. 8 Temperature field in the adhesive layer at holding time at t = 0 s (a) and t = 30s (b)

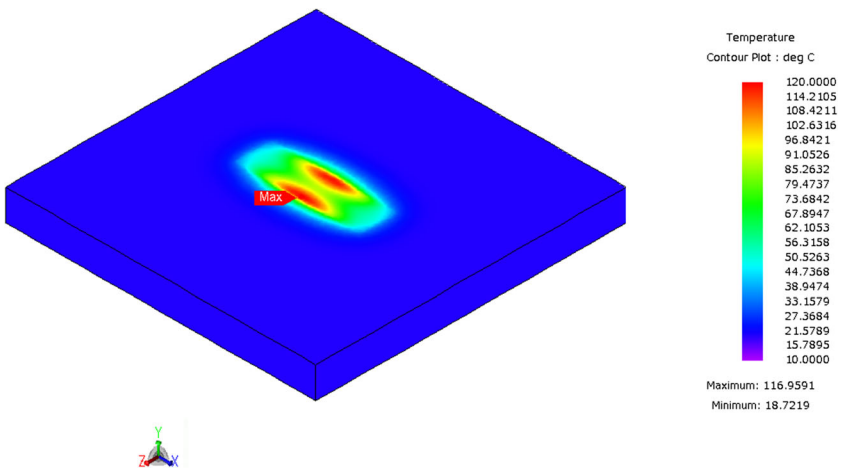

Fig. 9 Temperature field of Ertalon's support

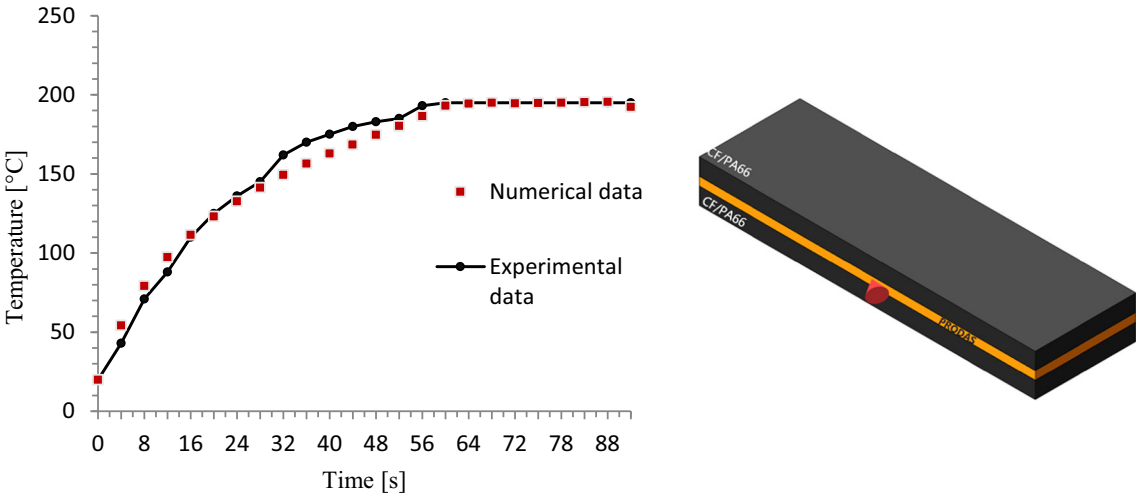

Fig. 10 Comparison of the numerical and experimental temperatures

It can be noted that for both the test methods, the highest values of strength occur for the same process parameter values, except for the holding time; in fact, in the case of short beam shear strength test, the maximum shear value is reached using a longer holding time than holding time used for the maximum shear value measured with the single lap joint shear test.

Table 3 Results of the short beam shear strength test and single lap joint shear test

I	T	t	Average D2344 (Mpa)	Average D5868 (Mpa)
I_1	T_1	t_1	16.413	0.451
I_1	T_1	t_2	17.790	0.876
I_1	T_1	t_3	19.928	0.844
I_1	T_2	t_1	20.041	1.156
I_1	T_2	t_2	22.339	1.435
I_1	T_2	t_3	20.079	1.323
I_1	T_3	t_1	20.698	1.198
I_1	T_3	t_2	22.339	1.206
I_1	T_3	t_3	22.107	1.203
I_2	T_1	t_1	20.884	0.740
I_2	T_1	t_2	22.546	1.058
I_2	T_1	t_3	21.767	0.887
I_2	T_2	t_1	19.688	0.892
I_2	T_2	t_2	20.352	1.506
I_2	T_2	t_3	20.698	1.505
I_2	T_3	t_1	21.972	1.471
I_2	T_3	t_2	21.796	1.486
I_2	T_3	t_3	21.610	1.496
I_3	T_1	t_1	21.045	1.029
I_3	T_1	t_2	18.197	0.876
I_3	T_1	t_3	19.780	0.930
I_3	T_2	t_1	20.677	2.086
I_3	T_2	t_2	26.465	1.435
I_3	T_2	t_3	22.359	1.323
I_3	T_3	t_1	19.575	1.743
I_3	T_3	t_2	23.184	1.765
I_3	T_3	t_3	22.858	1.789

This is explained by the fact that in the case of short beam shear strength test, the adhesion area is 480 mm^2, with a rectangular geometry, while in the case of single lap joint shear test, the adhesion area is 625 mm^2, with square geometry.

In the case of the rectangular geometry, the heating is more affected by the edge effect than the square one, as highlighted in Fig. 11.

Figure 12 shows the temperature distribution on the adherends for the process parameters 24 A, 195 °C and 30 s (Fig. 12(a)) and 10 A, 175 °C and 10 s (Fig. 12(b)). In the case of 30 s of holding time, the area of the temperature values close to 195 °C is very wide; this causes the squeezing of the melted adhesive and a degradation of the thermoplastic matrix of the adherends, lowering the strength of the joint, as evidenced by the experimental tests and shown in Fig. 13(c), where the joint realised with the process parameters of 24 A, 185 °C and 30 s is reported. Similarly, it is possible to highlight that in the case of holding time 10 s, the fusion of a large part of the adhesive is not obtained, especially towards the end of the joint. Also, in this case, the experimental tests show a lower strength of the joint. Moreover, it is possible to verify what has been highlighted also observing the extension of the adhesive fracture surface reported in Fig. 13b, relative to the case of holding time 10 s.

Finally, at the end of each test, the fracture surface of the joint was examined to evaluate the type of failure mode. In the

Table 4 Maximum values of shear strength for the short beam shear strength test and single lap joint shear test for induction-heated and reference samples

I	T	t	Average D2344 (MPa)	Average D5868 (MPa)
I_3	T_2	t_1	20.677	2.086
I_3	T_2	t_2	26.465	1.435
Reference sample			25.675	1.802

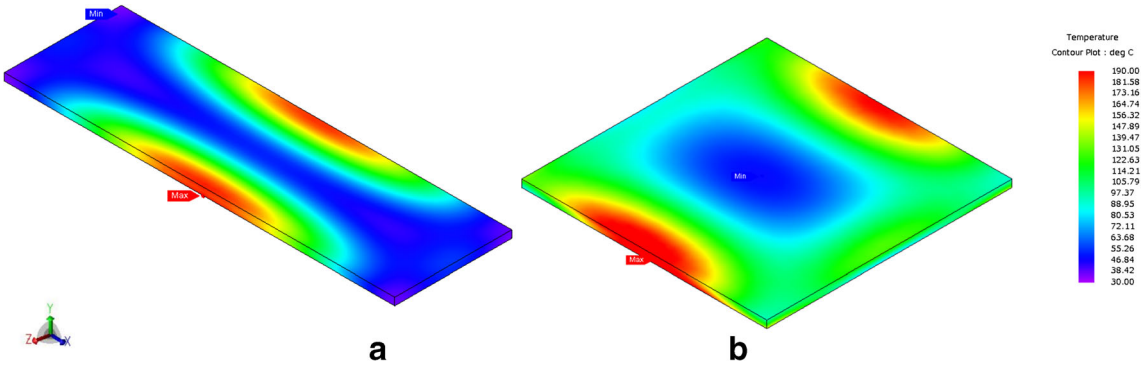

Fig. 11 Temperature distribution into the adhesive layer: **a** short beam shear strength and **b** single lap joint shear for the same process parameters: I_3, T_2 and t_2

case of the short beam shear strength test, failure also affects part of the adherend, specifically at the centre of the specimen, as shown in Fig. 13. In fact, the joints realised according to the short beam shear strength test are characterised by a fracture surface that does not affect only the adhesive layer but also the adherends. The adhesive-adherend interface shows higher strength for some values of the process parameters. In fact, in the case of the highest shear strength values (26.465 MPa), reported in Fig. 13(a), the fracture area affects only the adherends, meaning that the interface adhesive-adherends strength was the highest, realised with a current of 24 A, a maximum temperature of 185 °C and a holding time of 20s.

Figure 13(b) reports the joint realised with a current of 10 A, a maximum temperature of 175 °C and a holding time of 10 s, that is characterised by a shear strength value of 16.413 MPa. Analysing the fracture surface of this sample, it is possible to note that the value of the shear strength is lower than in the case of Fig. 13(a) depending on the adhesive fracture surface between adhesive and adherends.

Figure 14 shows that the joints realized according to the single lap joint shear test are characterised by a fracture area that does not affect only the adhesive layer but also the adhesive-adherend's interface. In the case of the highest shear strength values of the joint (2.086 MPa), the fracture area affects only the adhesive, meaning that the fracture was mostly cohesive, about 88% (Fig. 14(a)); the joint was realised with a current of 24 A, a maximum temperature of 185 °C and a holding time of 10s. In Fig. 14(b), the picture of the sample

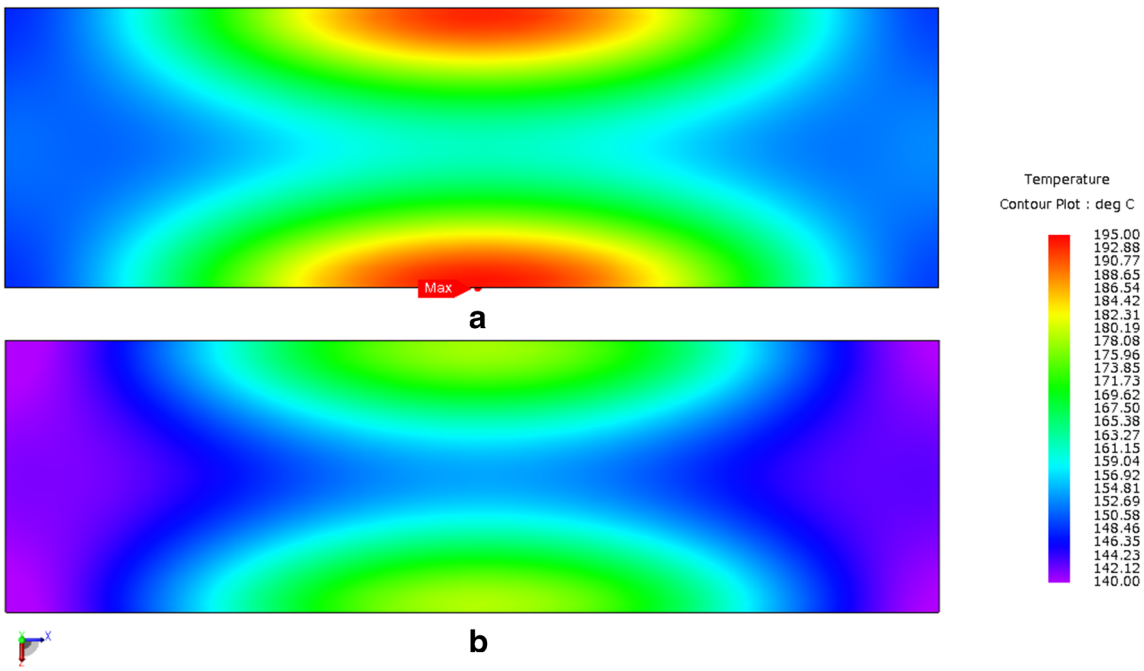

Fig. 12 Temperature distribution into the adhesive layer: **a** process parameters of 24 A, 195 °C and 30 s and **b** process parameters of 10 A, 175 °C and 10 s

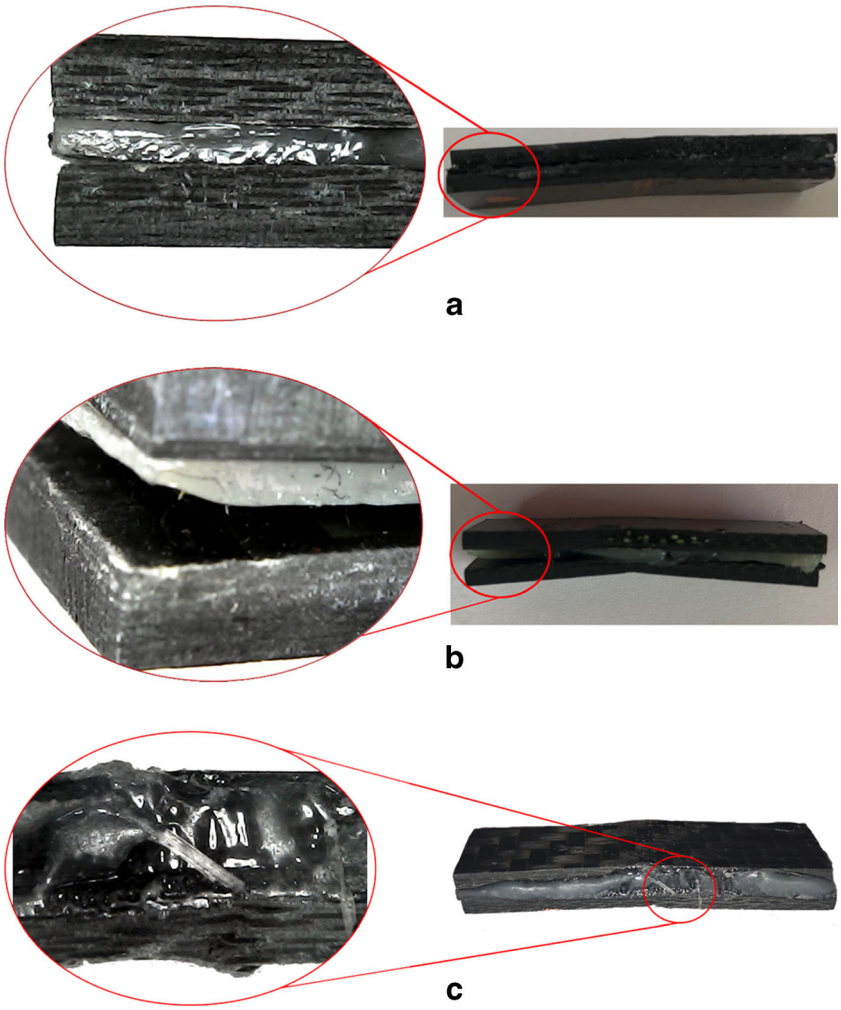

Fig. 13 Example of the fracture surface of short beam shear strength test: **a** adherend failure, **b** failure at the adhesive-adherend interface and **c** squeezing of the melted adhesive and degradation of the adherends

realised with 10 A, with a maximum temperature of 175 °C and a holding time of 10 s is shown. This sample is characterised by a shear strength value of 0.45 MPa, as highlighted by Fig. 14(b); it is primarily affected by an adhesive fracture surface, about 70%. The surface fracture was analysed using an image software, measuring the area highlighted in red and dividing it by the total overlap area.

5 Analysis of variance

After the mechanical test, the shear strength results were evaluated by analysis of variance (ANOVA). Firstly, a bar graph is reported, which considers all the average values of the shear stress obtained. Figure 14 and Fig. 15 show the trend of the strength stress as a function of the process parameters, such as holding time, temperature and current, for the two different ASTM standard methods adopted. In particular, it is evident how, in the case of short beam shear strength test, Fig. 14, the average value is less influenced by the process parameters adopted than the single lap joint shear test (Fig. 15). In fact, in this case, increasing the holding time, the temperature and the current, along with the horizontal axis, the shear strength increases.

The main effects plot provides for each factor the trend of the response or the influence of the factor on the response and the relative interaction between them.

A line joins all the average values of the factors: when the line is parallel to the X-axis, then there is no main effect; each value of the chosen variable affects the response in the same way, and the response average is the same for all values. When the line is not parallel to the X-axis, then there is the main effect, and different values of the considered variable affect the response differently. The higher the difference in the y coordinate of the points plotted, or the same, the line is not parallel to the X-axis, the higher the slope, and the higher the weight of the variable. For better understanding, dashed lines have been drawn that combine extreme values and give a quick idea of the resulting slope.

The graph reported in Fig. 16 shows how, in the case of the shear strength test standard, the three variables identified, such as the current, the temperature and the holding time, have a strong influence on the mechanical strength of the joint. This

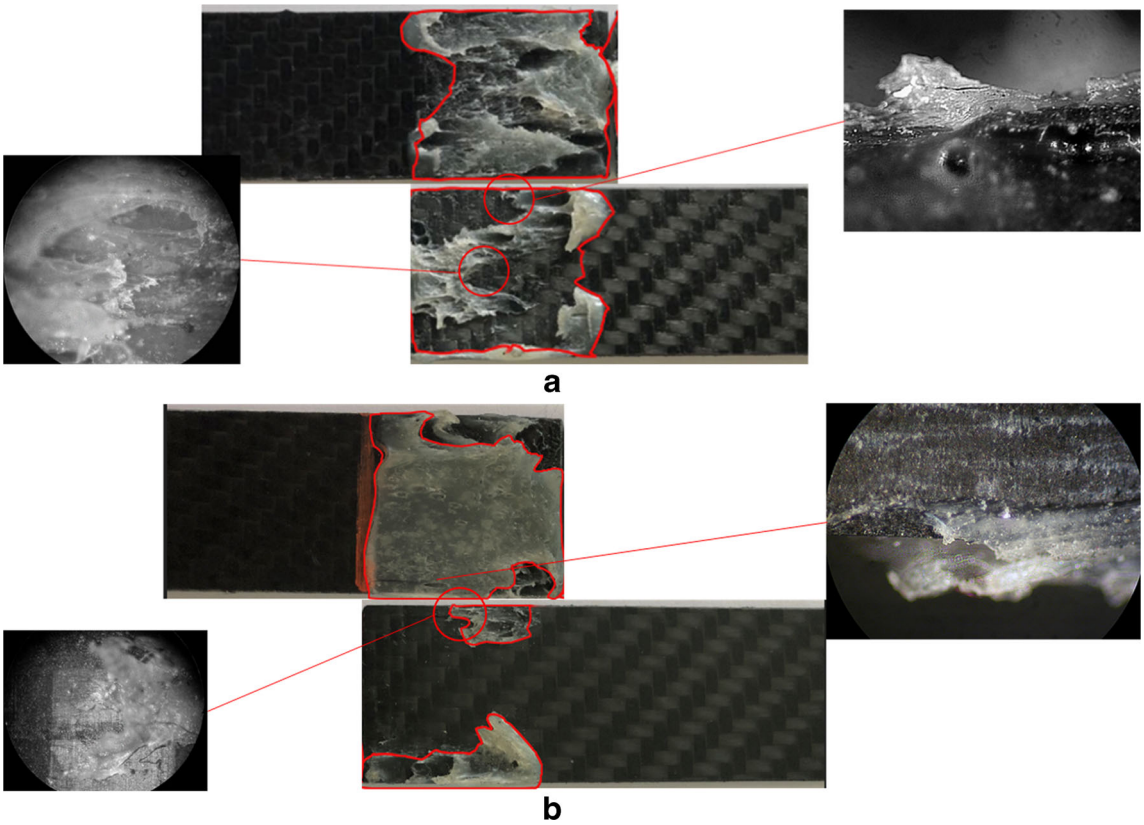

Fig. 14 Example of the fracture surface of single lap joint shear test: **a** cohesive failure, about 88%, and **b** adhesive failure, about 70%

also applies to the single lap joint shear test standard, even if in this case the effect of holding time concerning the other process parameters is less incident (Fig. 17).

The current and the temperature show an increasing linear trend; it is possible to see how increasing both the current value and the maximum temperature reached by the adhesive, the strength assumes increasing values, that is, re-enters in these cases of positive influence.

In the case of holding time, there is a parabolic trend with a downward concavity; however, in the presence of positive influence, from 10 to 20 s the value of the average load increases, but vice versa from 20 to 30 decreases. For this

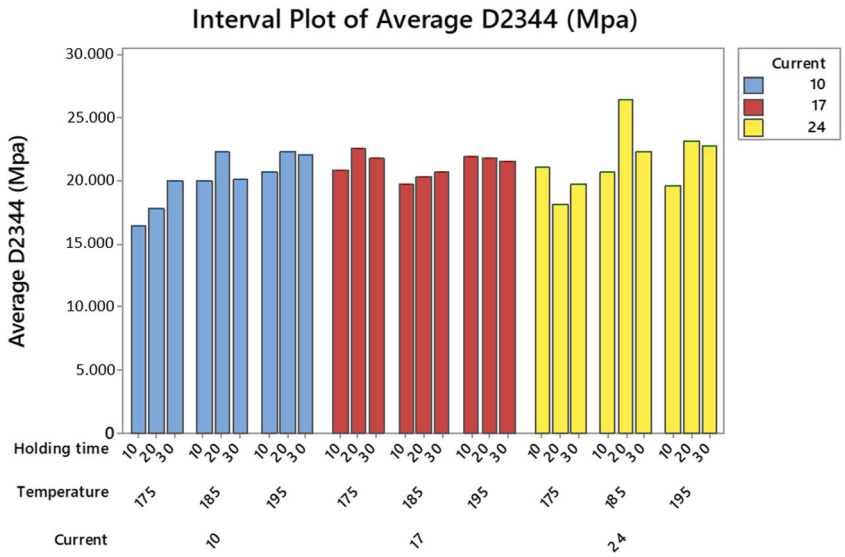

Fig. 15 Interval plot of average shear strength test

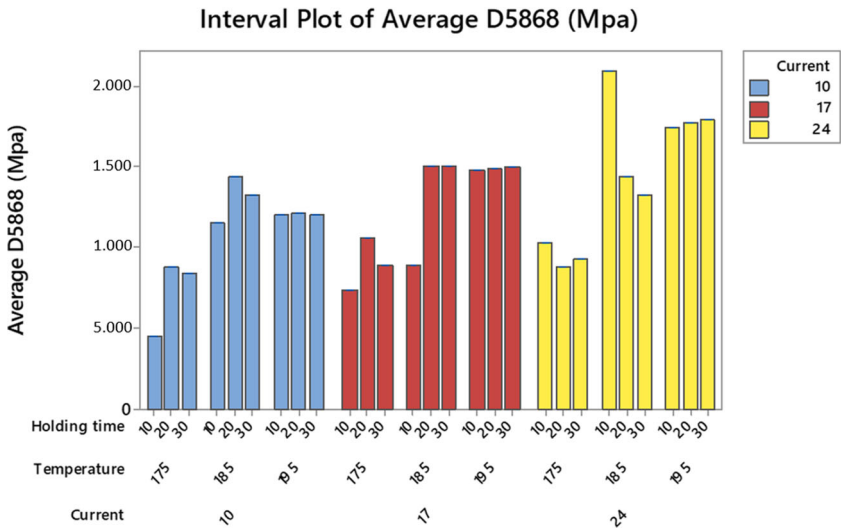

Fig. 16 Interval plot of average single lap joint shear test

reason, having chosen the interval 10 s-20 s-30 s has allowed envying the holding time value for which the maximum value for the shear stress is obtained. Choosing two levels instead of three and therefore only the 10 s-30 s interval would have allowed identifying the same the positive influence of the holding time on the task but would not allow identifying the maximum value, losing analytical information.

Additionally, in the case of the single lap joint shear test, it is possible to see how the effect of holding on joint strength is relatively less influential than the case of short beam shear strength test. The variation of strength is less than in the case of temperature, so time has less effect on the response parameter. This effect depends on the different configuration of the joint linked to the utilised normative. In fact, as already explained above, in the case of single lap joint shear test, the heating area is more extensive and with a square geometry; consequently, it is less affected by the edge effect, thus making the effect of holding time less effective; in fact, in the case of shear strength test, the effect of holding time is more significant.

6 Conclusions

This study investigates the curing behaviour and mechanical performance of electromagnetic induction-cured adhesive bonded joints of CFRTP composites, as a possible alternative to traditionally manual processes. The heat for liquefying the thermoplastic adhesive layer was generated in the adherends thanks to the presence of carbon fibre fabric.

It was used the Prodas 1400 thermoplastic adhesive as it is widely used in the automotive, industrial field.

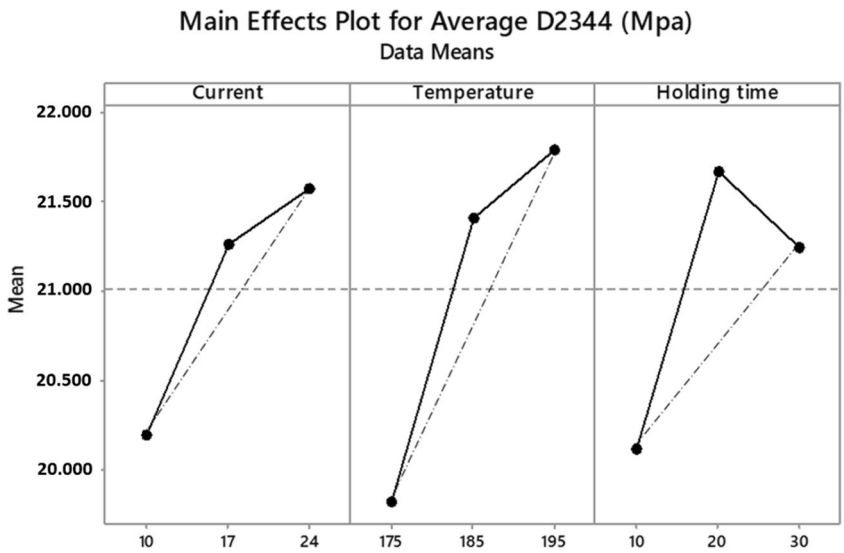

Fig. 17 Main effects plot for shear strength test results

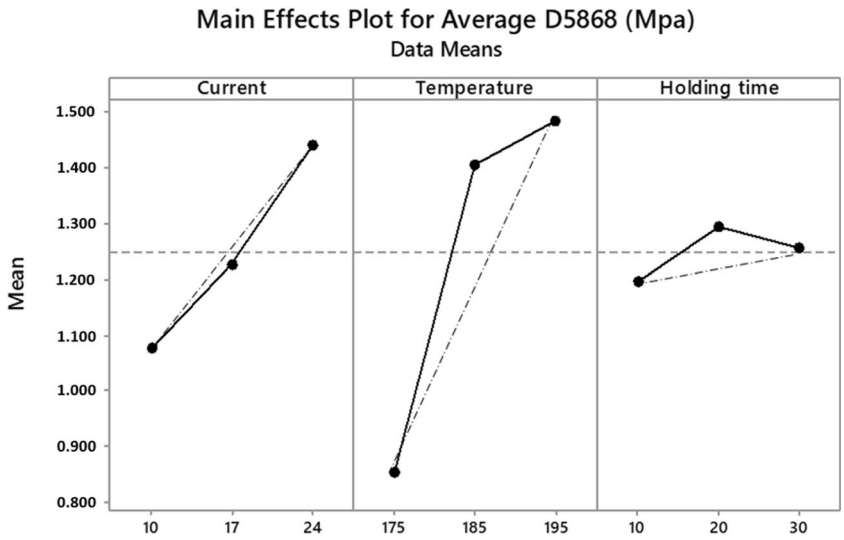

Fig. 18 Main effects plot for single lap joint shear test results

The results of numerical and experimental activities could be summarised as follows:

- A numerical model of induction heating has been proposed varying the process parameters such as current, maximum temperature and holding time.
- *The numerical simulation is useful for determining a suitable range of process parameters to obtain the melting of the adhesive on almost the whole contact area, avoiding both the adhesive squeezing and the lack of melting.*
- The temperature trend of the maximum temperature point provided by the numerical model is in excellent agreement with the experimental results.
- The holding time at a maximum temperature of the selected point is the key to obtain a more uniform temperature field that leads to the improvement of the joint mechanical strength.
- Curing the adhesive layer by the induction heating results in a slight increase in strength for both different configurations of joint studied, compared to the standard manual method.
- The analysis of variance has highlighted how both the current and the temperature increase the strength increase. Instead, in the case of holding time, the trend is parabolic with a downward concavity.
- *The proposed method allows to precisely control the temperature of the adhesive and in the adherends to avoid matrix degradation.* In a nutshell, induction heating could be a good alternative for curing hot-melt adhesive used for realising bonded joint of CFRTP, widely used in the automotive industry. The main advantage is the possibility of easy automation and the real-time control of temperature, instead of the traditional methods for which it is difficult to implement a correct temperature control of the adhesive.

Acknowledgements The authors would like to kindly acknowledge Dr. Francesco Galise of CRF (Fiat Research Center), Pomigliano d'Arco, Naples, Italy, for the technical support.

References

1. Hallal A, Elmarakbi A, Shaito A, El-Hage H (2013) Overview of composite materials and their automotive applications. In: Advanced composite materials for automotive applications. Wiley, Chichester, pp 1–28
2. Ageorges C, Ye L, Hou M (2001) Advances in fusion bonding techniques for joining thermoplastic matrix composites: a review. Compos Part A Appl Sci Manuf 32:839–857. https://doi.org/10.1016/S1359-835X(00)00166-4
3. Teti R (2002) Machining of composite materials. CIRP Ann 51:611–634. https://doi.org/10.1016/S0007-8506(07)61703-X
4. Sheikh-Ahmad JY, Almaskari F, Hafeez F (2019) Thermal aspects in machining CFRPs: effect of cutter type and cutting parameters. Int J Adv Manuf Technol 100:2569–2582. https://doi.org/10.1007/s00170-018-2881-1
5. Skeist I (2012) Handbook of adhesives. Springer Science & Business Media, Berlin
6. Leone C, Genna S (2018) Effects of surface laser treatment on direct co-bonding strength of CFRP laminates. Compos Struct 194:240–251. https://doi.org/10.1016/J.COMPSTRUCT.2018.03.096
7. Pizzorni M, Lertora E, Gambaro C, Mandolfino C, Salerno M, Prato M (2019) Low-pressure plasma treatment of CFRP substrates for epoxy-adhesive bonding: an investigation of the effect of various process gases. Int J Adv Manuf Technol 102:3021–3035. https://doi.org/10.1007/s00170-019-03350-9
8. Haimbaugh RE (2015) Practical induction heat treating. ASM International, Cleveland
9. Sergio Lupi, Michele Forzan, Aleksandr Aliferov (2015) Induction and Direct Resistance Heating
10. Miller AK, Chang C, Payne A, Gur M, AP EM (1990) The nature of induction heating in graphite–fiber, polymer–matrix composite materials. SAMPE J 26:37–54
11. Fink BK, McCullough RL, Gillespie JW (2004) A local theory of heating in cross-ply carbon fiber thermoplastic composites by

magnetic induction. Polym Eng Sci 32:357–369. https://doi.org/10.1002/pen.760320509
12. Yarlagadda S, Kim HJ, Gillespie JW et al (2002) A study on the induction heating of conductive fiber reinforced composites. J Compos Mater 36:401–421. https://doi.org/10.1177/0021998302036004171
13. Sánchez Cebrián A, Zogg M, Ermanni P (2013) Methodology for optimization of the curing cycle of paste adhesives. Int J Adhes Adhes 40:112–119. https://doi.org/10.1016/j.ijadhadh.2012.09.002
14. Severijns C, de Freitas ST, Poulis JA (2017) Susceptor-assisted induction curing behaviour of a two component epoxy paste adhesive for aerospace applications. Int J Adhes Adhes 75:155–164. https://doi.org/10.1016/j.ijadhadh.2017.03.005
15. Gouin O'Shaughnessey P, Dubé M, Fernandez Villegas I (2016) Modeling and experimental investigation of induction welding of thermoplastic composites and comparison with other welding processes. J Compos Mater. https://doi.org/10.1177/0021998315614991
16. Chadegani A, Batra RC (2011) Analysis of adhesive-bonded single-lap joint with an interfacial crack and a void. Int J Adhes Adhes 31:455–465. https://doi.org/10.1016/J.IJADHADH.2011.02.006
17. Luo Q, Tong L (2009) Analytical solutions for nonlinear analysis of composite single-lap adhesive joints. Int J Adhes Adhes 29:144–154. https://doi.org/10.1016/J.IJADHADH.2008.01.007
18. da Silva LFM, das Neves PJC, Adams RD, Spelt JK (2009) Analytical models of adhesively bonded joints—part I: literature survey. Int J Adhes Adhes 29:319–330. https://doi.org/10.1016/J.IJADHADH.2008.06.005
19. de Castro J, Keller T (2008) Ductile double-lap joints from brittle GFRP laminates and ductile adhesives, part I: experimental investigation. Compos Part B Eng 39:271–281. https://doi.org/10.1016/J.COMPOSITESB.2007.02.015
20. Reis PNB, Ferreira JAM, Antunes F (2011) Effect of adherend's rigidity on the shear strength of single lap adhesive joints. Int J Adhes Adhes 31:193–201. https://doi.org/10.1016/J.IJADHADH.2010.12.003
21. Pahr DH, Rammerstorfer FG, Rosenkranz P et al (2002) A study of short-beam-shear and double-lap-shear specimens of glass fabric/epoxy composites. Compos Part B Eng 33:125–132. https://doi.org/10.1016/S1359-8368(01)00063-4
22. Precision WS (2011) Standard test method for short-beam strength of polymer matrix composite materials. Annu B ASTM Stand 00:1–8. https://doi.org/10.1520/D2344
23. Specimen J, Results T (2005) ASTM D5868 standard test method for lap shear adhesion for fiber reinforced plastic (FRP). Reproduction 01:4–5. https://doi.org/10.1520/D5868-01R14.2
24. Ahmed TJ, Stavrov D, Bersee HEN, Beukers A (2006) Induction welding of thermoplastic composites—an overview. Compos Part A Appl Sci Manuf 37:1638–1651. https://doi.org/10.1016/J.COMPOSITESA.2005.10.009
25. Li X, Strieder W (2009) Emissivity of high-temperature fiber composites. Ind Eng Chem Res 48:2236–2244. https://doi.org/10.1021/ie8008583
26. Kranjc M, Zupanic A, Miklavcic D, Jarm T (2010) Numerical analysis and thermographic investigation of induction heating. Int J Heat Mass Transf 53:3585–3591. https://doi.org/10.1016/J.IJHEATMASSTRANSFER.2010.04.030